JOURNAL OF SOLID STATE CHEMISTRY **141,** 330–337 (1998)
ARTICLE NO. SC987929

Mechanism of Host-Layer Restacking in Hg_xTiS_2

Max V. Sidorov,*,† Michael J. McKelvy,*,†,[1] Renu Sharma,*,† and William S. Glaunsinger*,†,‡

*Center for Solid State Science, †Science and Engineering of Materials Graduate Program, and ‡Department of Chemistry and Biochemistry, Arizona State University, Tempe, Arizona 85287

Received February 12, 1998; in revised form June 11, 1998; accepted June 15, 1998

High-resolution transmission electron microscopy has been used to observe the host-layer restacking process *in situ* during Hg_xTiS_2 ($1.24 \geq x \geq 0.00$) deintercalation to better understand the role of elastic strain in reaction dynamics and phase formation for this low-valent system ($Hg^{\delta+}$, $\delta \ll 1$). Hg forms novel incommensurate one-dimensional guest chains that occupy channels between the host layers. These channels undergo trigonal prismatic (TP)-to-distorted trigonal antiprismatic (DTAP) coordination restacking during deintercalation. Initially, a small metastable TP-coordinated, empty-gallery region forms. This region usually undergoes rapid restacking to octahedral coordination (1T-TiS_2), which induces an intragallery TP-to-DTAP Hg_xTiS_2 phase transition to minimize elastic host-layer strain. Occasionally, TP empty-gallery regions become too large to allow coherent gallery restacking, resulting in host-layer fault/crack formation. TP and DTAP intercalate lamella can readily form coherent lamellar intergrowths, resulting in lamellar mixed-phase regions forming during deintercalation. © 1998 Academic Press

INTRODUCTION

Layered transition-metal dichalcogenides (TMDs), such as 1T-TiS_2, are well known for their ability to form intercalation compounds with a wide variety of guests, including metals (1,2). Metal guests generally occupy specific lattice sites in the expanded host lattice and exhibit substantial guest–host charge transfer. However, recent studies have shown that mercury-intercalated TiS_2 exhibits novel properties not found in other metal-intercalated TMDs (3–12). These properties include superstoichiometric mercury uptake (Hg_xTiS_2, $0.00 \leq x \leq 1.24$), essentially no guest-host charge transfer, complete thermal reversibility of the intercalation process, and the formation of infinite incommensurate mercury chains in the host galleries. Detailed structural analysis of Hg_xTiS_2 has shown this compound to have an unusual (3 + 1)-dimensional structure (10,11), which is best described by interpenetrating TiS_2 and Hg monoclinic sublattices, with common a and c axes, incommensurate b axes parallel to the Hg chains, and the layer stacking direction along c^*.

Hg_xTiS_2 can exist in two similar monoclinic structures, $\beta = 102^\circ$ [$a = 5.92$ Å, $b(TiS_2) = 3.41$ Å, $b(Hg) = 2.76$ Å, $c = 8.86$ Å, and $\beta = 102.3^\circ$] and $\beta = 96^\circ$ [$a = 5.92$ Å, $b(TiS_2) = 3.41$ Å, $b(Hg) = 2.76$ Å, $c = 8.70$ Å, and $\beta = 96.5^\circ$] modifications. These modifications only differ by a minor shift ($\frac{1}{2}\mathbf{b}$) of the host layers along the incommensurate Hg chains (10,11) and can coherently intergrow as distinct lamellar regions within the same crystal, as shown in Fig. 1. The in-plane structure of the host and guest layers is the same for both modifications. Evidence for such intergrowths has recently been discovered by high-resolution transmission electron microscopy (HRTEM), where $\frac{1}{2}\mathbf{b}$ shifts of the host layers were occasionally observed along the a-axis direction, consistent with the presence of $\frac{1}{2}\mathbf{b}$ stacking faults (11). The primary structural difference between the phases is the coordination of the sulfur channels surrounding the Hg chains, which is trigonal prismatic (TP) for the $\beta = 102^\circ$ phase and distorted trigonal antiprismatic (DTAP) for the $\beta = 96^\circ$ phase. The free energy difference between the two phases is subtle, with the 102° phase being observed for the fully intercalated stage-1 intercalate, $Hg_{1.24}TiS_2$, and the 96° phase found for partially deintercalated Hg_xTiS_2 (10, 11). These observations suggest an intriguing low-energy phase transition occurs during deintercalation. In this study, we follow the dynamic atomic-level deintercalation process *in situ* using HRTEM to investigate individual guest-gallery/host-layer behaviors and their role in the associated phase transition mechanisms.

EXPERIMENTAL

Stage-1 $Hg_{1.24}TiS_2$ was prepared by reaction of stoichiometric amounts of high-purity Hg (<5 ppm metal impurities) and TiS_2 at 320°C, followed by slow cooling to ambient temperature, as reported previously (3–5). Highly stoichiometric TiS_2 ($Ti_{1.002}S_2$) was prepared by direct reaction of the elements. The host was compositionally and structurally characterized by oxidative thermogravimetric

[1]To whom correspondence should be addressed.

0022-4596/98 $25.00

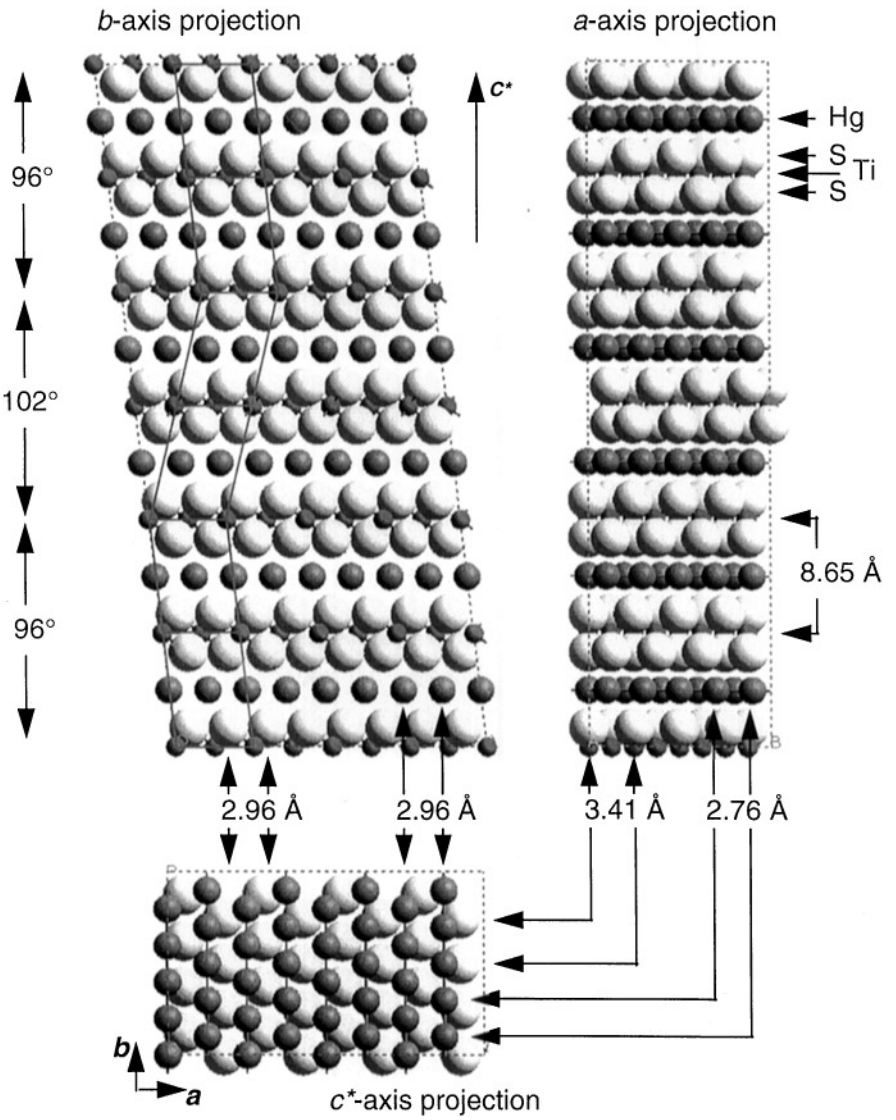

FIG. 1. Model of a six-layer region of Hg_xTiS_2 showing coherent intergrowth of the 102° and 96°-Hg_xTiS_2 structures, with two layers of the 102° structure surrounded by a 96°-structure matrix. Such coherent intergrowths can be formed during the 102°-to-96° phase transition by $\frac{1}{2}\mathbf{b}$ shifts of the host layers associated with the 102° phase. Projections along the Hg chains (*b* axis), perpendicular to the in-plane chain direction (*a* axis), and perpendicular to the layers (*c** axis) are shown together with their interrelationships. The projection perpendicular to the host layers shows the relationship between individual Hg and sulfur layers for clarity.

analysis and X-ray powder diffraction (XPD), respectively (13, 14). Intercalate sample compositions ($Hg_{1.24\pm0.01}TiS_2$) were determined by thermogravimetric analysis (TGA) of the complete deintercalation process under an argon atmosphere (5).

HRTEM samples were prepared by crushing the intercalate at -196°C in a nitrogen-containing glovebox, followed by warming the freshly crushed crystallites to ambient temperature and dispersing them on holey-carbon-coated copper TEM grids. XPD and TGA compositional analysis confirmed that no significant structural or compositional change occurred during sample preparation (4, 5, 9).

The HRTEM investigations were performed under ambient microscope conditions. Both Topcon 002B [200 kV, spherical aberration coefficient (C_s) $\approx$ 0.4 mm, and a point-to-point resolution of 1.8 Å] and JEOL 4000FX [400 kV, $C_s \approx 1.0$ mm, and a point-to-point resolution of 1.7 Å] transmission electron microscopes were used in this investigation. Some deintercalation occurs upon sample exposure to the microscope vacuum, so the samples observed inherently experience some deintercalation prior to

observation. Electron beam heating was used to further stimulate the deintercalation process and facilitate dynamic observations of individual-gallery deintercalation behavior. HRTEM observations were made parallel to the host layers to elucidate the structural behavior of individual galleries and their adjacent host layers during deintercalation. The observed time for individual-gallery deintercalation ranged from complete deintercalation in less than a second to galleries that never completely deintercalated (e.g., residue compounds). Careful control of electron beam sample heating was necessary to achieve suitable rates for *in situ* HRTEM observations. Crystal orientations and distances were determined by combined direct-lattice and Fourier-transform measurements (11,15). Image processing was performed using an image analysis software application package (Digital Micrograph) installed on a Quadra 950 Macintosh computer. This package provides many tools for analysis and processing of HRTEM images, including Fourier filtering (16).

RESULTS

Structural factors

Although the experimental images of the 102° and 96° structures are indistinguishable along their *a*- and *b*-axis projections (11), significant insight into the 102°-to-96° phase transition can be gained by HRTEM observations of individual-gallery and host-layer behavior during deintercalation. This follows, in part, from the lamellar nature of the phase transition, which suggests individual intercalate lamella can undergo the transition independent of the structure of their neighboring lamellar phase(s), as shown in Fig. 1.

Most often, individual-gallery deintercalation was observed to progress from side to side across sample crystals, as opposed to front to back/back to front or some combination of the two. This behavior was generally independent of the crystal's plane-parallel crystallographic orientation (e.g., viewed along *a* or *b*) and can be associated with the physical dimensions of the sample crystals, which are inherently thinner from front to back (e.g., limited to a few hundred Angstroms in thickness for HRTEM imaging) than from side to side.

As deintercalation progresses across a gallery, the crystal becomes elastically strained due to the bending of the host layers about the guest-edge dislocation (GED) termination that separates the intercalated and deintercalated regions of the gallery. This strain energy contributes to the activation energy needed for deintercalation, with more extensive GED fronts requiring a higher activation energy. Consequently, less activation energy is required to form GED deintercalation fronts that travel from side to side across the HRTEM crystals, as they minimize the elastic strain energy associated with deintercalation. As a result, the majority of the galleries observed deintercalated across the field of view.

Intercalate Hg chains have previously been observed to exhibit substantial thermally induced disorder along *b* (11), indicating deintercalation generally occurs via diffusion of the Hg chains along their chain-axis direction. Since side-to-side deintercalation is observed for crystals independent of their plane-parallel orientation with the electron beam, the crystal's morphology, rather than its Hg-chain orientation, appears to be the primary factor in producing the observed side-to-side GED progression during deintercalation.

The possible in-plane shifts for the TP ($Hg_{1.24}TiS_2$, 102° phase)-to-octahedral (TiS_2) restacking of the galleries during deintercalation are shown in Fig. 2. Restacking can occur either via combined host-layer shifts of $\frac{1}{2}\mathbf{b} + \frac{1}{6}\mathbf{a}$ or by a direct shift of $-\frac{1}{3}\mathbf{a}$. The former process involves both TP-to-DTAP ($\frac{1}{2}\mathbf{b}$) and DTAP-to-octahedral ($\frac{1}{6}\mathbf{a}$) components, whereas the latter process involves direct TP-to-octahedral ($-\frac{1}{3}\mathbf{a}$) restacking and does not accommodate intermediate DTAP stacking. TP-to-DTAP intercalate host-layer restacking along **b** is a relatively low-energy process, with the host layers gliding along the Hg chains between comparable energy levels. Intercalate host-layer restacking motion along **a** is expected to be more difficult, since it requires host-layer motion perpendicular to the chains (Fig. 1).

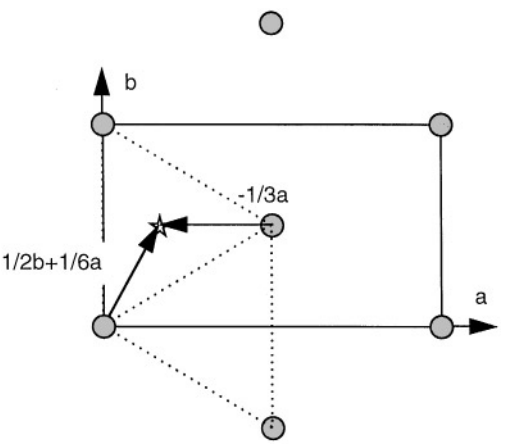

FIG. 2. A vector diagram showing the two possible host-layer restacking shifts that can accomplish the intragallery TP-to-octahedral gallery coordination shift that accompanies $Hg_{1.24}TiS_2$ (102° phase) deintercalation to TiS_2. The $\frac{1}{2}\mathbf{b} + \frac{1}{6}\mathbf{a}$ process has a vector component ($\frac{1}{2}\mathbf{b}$) which, as a first step, results in intermediate DTAP restacking (e.g., via the 102°-to-96° phase transition in Hg_xTiS_2) that takes advantage of the low energy requirements for host-layer restacking along the Hg chains. The analogous vector shift ($-\frac{1}{2}\mathbf{b} + \frac{1}{6}\mathbf{a}$) can similarly accomplish the observed $Hg_{1.24}TiS_2$ (102° phase)-to-TiS_2 restacking shift. The direct $-\frac{1}{3}\mathbf{a}$ shift can also achieve the overall restacking process, but does not involve intermediate DTAP restacking.

Simple Gallery Restacking

Individual-gallery deintercalation was usually observed to involve adjacent fully intercalated (8.7-Å interlayer spacing) and fully collapsed (5.7-Å interlayer spacing) regions, as shown in Fig. 3. The fully intercalated spacing is consistent with either the 102° or 96° intercalate structure, as described previously. The fully collapsed spacing is in good agreement with the octahedral empty-gallery packing in TiS_2 (5.695-Å interlayer spacing) (17), the thermal deintercalation product (5,11). Figures 3a and 3b show deintercalating Hg GEDs viewed close to their *a* and *b* directions, respectively. The 3-Å interlayer transitions between the neighboring intercalated and empty-gallery regions are separated by only ~20 Å laterally across the GED termination sites for either the *a* or *b* crystal orientation. Narrow transition regions of this type were commonly observed for both orientations. Such processes are consistent with DTAP (96° – Hg_xTiS_2 phase)-to-octahedral (TiS_2) restacking transitions, which only require a $\frac{1}{6}\mathbf{a}$ shift (1 Å) across the intragallery boundary, which minimizes the elastic host-layer strain induced by the transition. The near symmetry and the asymmetry of the host layers that surround the GED terminations viewed along *a* and *b*, respectively, suggest modest host-layer restacking along *a* (≤ 1 Å) occurs across the boundary, consistent with an intragallery transition from the 96°-Hg_xTiS_2 phase to TiS_2. Significantly greater in-plane host-layer shifts (i.e., 2 Å) would be needed for a direct TP (102°-Hg_xTiS_2

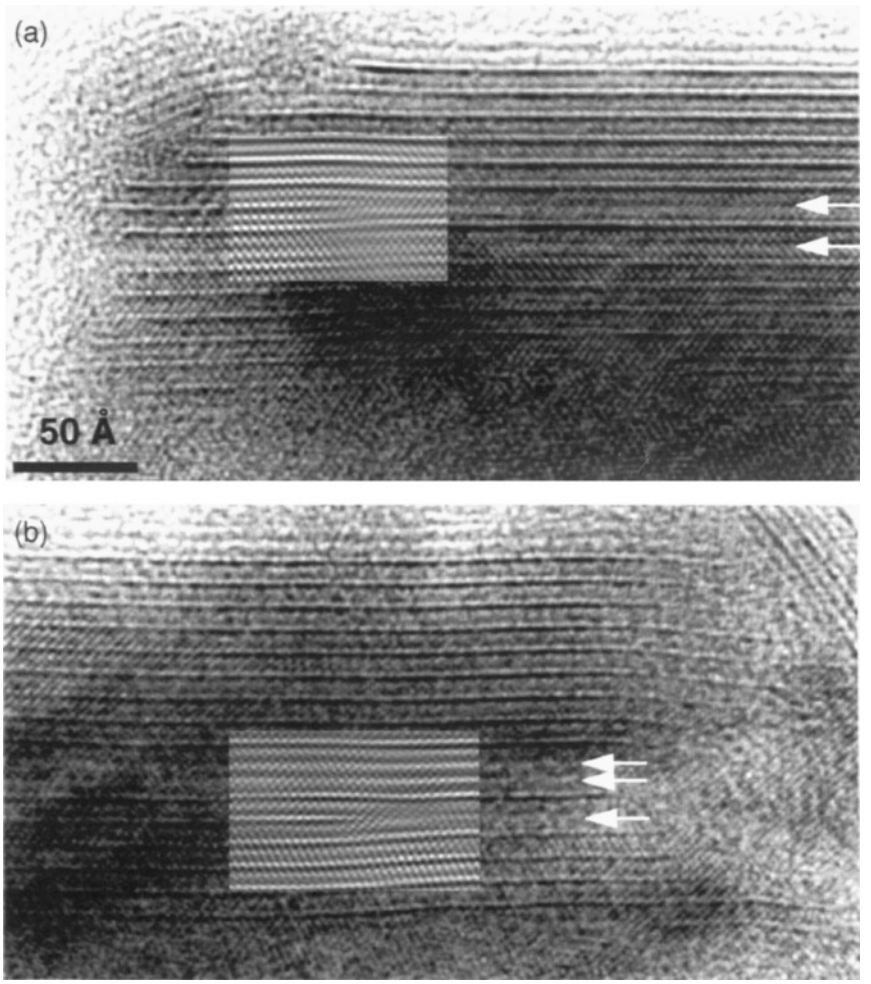

FIG. 3. HRTEM images of Hg_xTiS_2 crystals showing typical GED behavior during individual gallery deintercalation. The crystals in (a) and (b) are viewed close to their *a* and *b*-axis directions, respectively. Their deintercalating galleries have adjacent 8.7- and 5.7-Å regions which are separated by only ~20 Å, which is typically observed during individual gallery deintercalation. These observations are consistent with the DTAP-to-octahedral gallery coordination transition expected for the 96°-Hg_xTiS_2-to-TiS_2 intragallery transition. Note the near symmetry of the host layers about the GED termination in (a) and the asymmetry of the host layers immediately above and below the GED termination in (b). The narrow dark lines with the strongest contrast represent the Hg layers. The white arrows indicate both the deintercalating galleries and other galleries that have already deintercalated. The inserted regions containing the GED terminations have been Fourier filtered, as in previous studies (11).

phase)-to-octahedral (TiS_2) intragallery transition. The foregoing observations are also consistent with the observed formation of the 96°-Hg_xTiS_2 phase early in the deintercalation process (11).

Complex Restacking with Defect Formation

HRTEM studies of the early stages of individual-gallery deintercalation occasionally revealed a more complex restacking process, as shown in Fig. 4. Figure 4a shows an extensive stage-1 region of a relatively large Hg_xTiS_2 crystal viewed close to the *b* direction. Deintercalation onset occurs in the upper indicated gallery, with the resulting GED termination forming at the right side of the crystal and progressing from right to left together with Hg deintercalation, as shown in Figs. 4b–e. Close examination of the early deintercalation behavior of the gallery (Fig. 4b shows the process a few seconds after its onset) indicates the

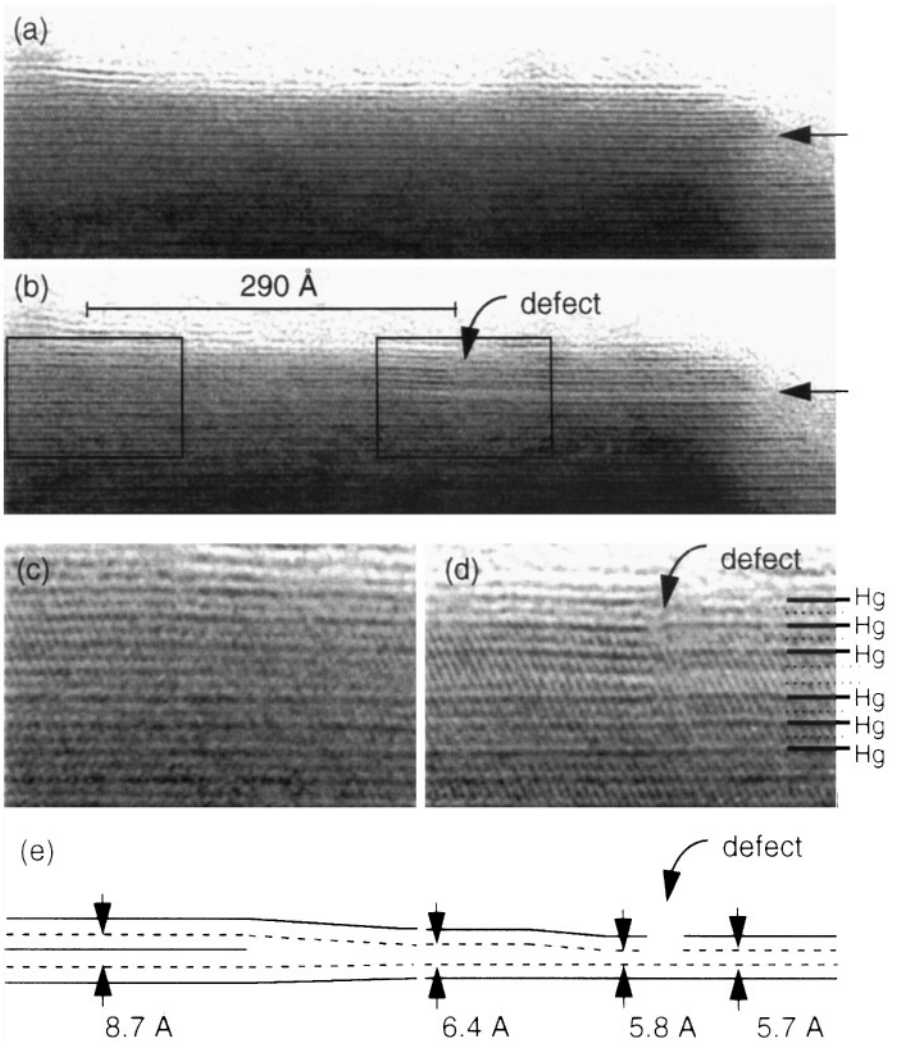

FIG. 4. HRTEM observation of individual GED formation, progression, and the delayed host-layer collapse of its trailing empty-gallery region during deintercalation (viewed close to [010]). The narrow dark lines with the strongest contrast represent the Hg layers. The image in (a) shows the fully intercalated crystal. (b) An upper guest layer [indicated by the black arrows to the right in both (a) and (b)] forms a GED termination at the right of the crystal, which begins to migrate to the left with guest-layer deintercalation. An interlayer defect nearly perpendicular to the host layers forms during the process, as indicated by the curved arrow. The image in (c) is a magnified region of (b) showing the GED termination, whereas (d) is a magnified region of (b) showing the region containing the interlayer defect; (e) is a schematic depiction of the deintercalating gallery shown in (c) and (d). The solid and dashed lines represent the Hg and Ti layers, respectively. The position of the interlayer defect is indicated by the partially separated upper TiS_2 and Hg layers to the right. Representative interlayer measurements from the four regions of the gallery are shown at their measurement sites. From left to right, the first through fourth regions have 8.7 Å (intercalated region containing the GED), 6.4 Å (to the right of the intercalate region after a transition region), 5.8 Å (immediately to the left of the interlayer defect), and 5.7 Å (to the right of the defect) interlayer repeats. The interlayer spacings across each region were constant within experimental error ($\pm$ 0.2 Å), except for region 2, which measured 6.4 $\pm$ 0.3 Å.

empty-gallery region laterally trailing the GED termination takes ~290 Å to achieve the known defect-free interlayer spacing for TiS_2 (5.7 Å) (13,14). Such delayed recovery of the octahedral host-layer spacing suggests a relatively complex host-layer restacking mechanism. The gallery undergoing deintercalation in Figure 4 can be described in terms of four regions from left to right: (i) a fully intercalated region to the left of the GED termination, with an interlayer spacing of 8.7 Å; (ii) a transition to a second, partially collapsed, deintercalated region, with a slightly variable interlayer spacing of 6.4 ± 0.3 Å, depending on the location; (iii) a relatively brief transition to a short third region with an interlayer spacing of 5.8 Å just before the interlayer defect; and (iv) a fully collapsed region, with an interlayer spacing of 5.7 Å, to the right of the defect.

These regions can be directly related to the host-layer restacking process. The interlayer spacings for the regions are in good agreement with the interlayer spacings expected for (i) a fully intercalated gallery of the 102° structure with TP gallery coordination, (ii) a transition to TP coordination of a relatively wide empty-gallery region, (iii) a coordination transition to a narrow DTAP region between the second region and the interplanar defect (the expected host-layer spacings for TP and DTAP coordination of the empty- gallery regions are 6.3 and 5.8 Å, based on the sulfur–sulfur distances in TiS_2) (17), and (iv) octahedral TiS_2 coordination of the gallery to the right of the defect.

The 102°- and 96°-intercalate structures cannot be distinguished directly for region i, as their *b*-axis images are indistinguishable (11). However, the good interlayer distance match of region ii with empty-gallery TP coordination indicates host-layer restacking has not yet occurred in region ii, so that the 102°-intercalate structure is likely still present in region i. The restacking process to the right of the TP empty-gallery region is rather complex and cannot be definitively assigned due to the small difference in the interlayer spacings between DTAP and octahedral packing (0.1 Å), which is within experimental error (± 0.2 Å). The region to the right of the defect (region iv) is likely an octahedrally coordinated, empty-gallery TiS_2 region, formed via the interlayer defect between regions iii and iv. The defect visibly disrupts the host layers above the gallery, allowing the required octahedral restacking shift of the upper host layer associated with region iv along *a*.

Most likely, the restacking process involving regions iii and iv begins with a restacking shift along *b*, inducing intralayer stress in the right side of the relatively large empty-gallery region. To complete the TP-to-octahedral restacking process in region iv, the interlayer defect then forms to provide the requisite $\frac{1}{6}\mathbf{a}$ interlayer shift of the upper host layer region to the right of the defect. Region iii is likely a $\frac{1}{2}\mathbf{b}$ residual transition region from TP to DTAP or near-DTAP coordination (consistent with an expected interlayer spacing shift from 6.3 to 5.8 Å), with the interlayer defect required for the remaining $\frac{1}{6}\mathbf{a}$ interlayer shift to octahedral TiS_2.

As discussed previously, TP-to-octahedral restacking may also occur via a $-\frac{1}{3}\mathbf{a}$ restacking shift of the upper host layer. However, such a restacking process is not plausible in Fig. 4, since a negative (2 Å) *a*-axis shift of the right region of the upper host layer into the left region is not energetically reasonable. Since such delayed empty-gallery restacking was rarely observed, it appears that this process is not generally representative of the primary deintercalation process, but may contribute to stacking fault and/or defect formation associated with the process.

DISCUSSION

Simple Restacking Mechanism

The foregoing observations lead to a general model for the primary Hg_xTiS_2 gallery deintercalation process and the associated 102°-to-96° phase transition, as shown in Fig. 5. Initially, a GED termination forms at the end of the gallery and begins to progress into the gallery with deintercalation. As the trailing empty-gallery region forms, it initially adopts the TP stacking of the 102°-$Hg_{1.24}TiS_2$ structure to minimize local stress, as shown in Fig. 5b. As the area of the empty-gallery region grows, so does the driving force for host-layer restacking. The empty-gallery and intercalate regions usually undergo host-layer restacking to the octahedral stacking of TiS_2 and DTAP stacking of the 96°-Hg_xTiS_2 phase early in the gallery deintercalation process. This involves a coherent $\frac{1}{2}\mathbf{b}$ shift of the surrounding host layers (Fig. 5c) together with a $\frac{1}{6}\mathbf{a}$ shift between the intercalate and empty-gallery regions, which can be facilitated, at least in part, by asymmetry of the host layers about the GED termination along its *a* direction (Fig. 5d). Since the expected interlayer spacings for DTAP and octahedral empty-gallery coordination only differ by 0.1 Å (5.8 vs 5.7 Å), which is within the accuracy of our HRTEM measurements (± 0.2 Å), the precise position of this coordination transition is uncertain and the complete transition region could extend beyond the observed ~20-Å transition widths into the empty region of the gallery. However, short intragallery Hg_xTiS_2-to-TiS_2 coordination transitions should be preferred, since they can better accommodate the requisite host-layer restacking across the transition via surrounding host-layer asymmetry along *a*. This model explains the 102°-to-96°Hg_xTiS_2 phase transition, which occurs early in the $Hg_{1.24}TiS_2$ deintercalation process. It also highlights the potential importance of elastic strain in intercalate phase formation, in addition to its prominent role in intercalation and deintercalation processes (11,18,19).

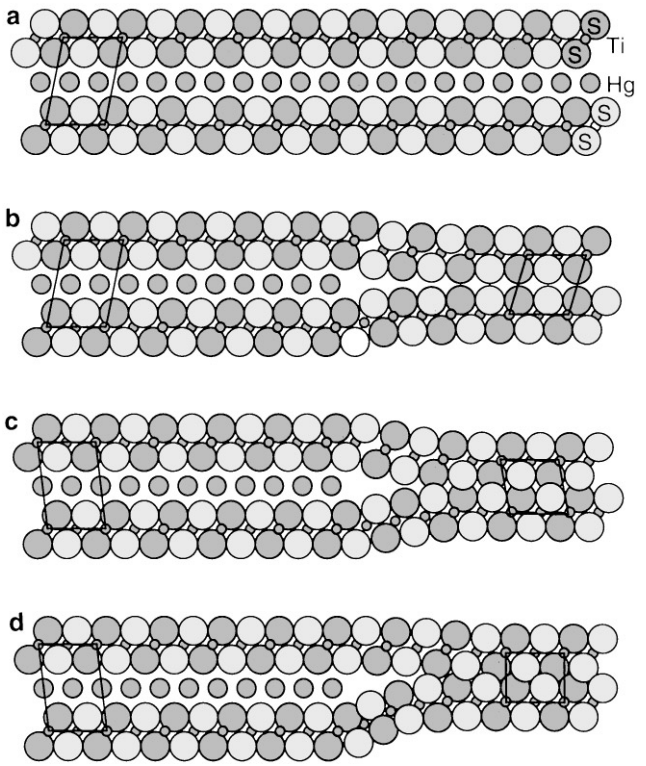

FIG. 5. A model of the host-layer restacking process and the 102°-to-96° Hg_xTiS_2 phase transition induced by Hg_xTiS_2 deintercalation viewed along *b*. The arrangement in (a) shows a single intercalate layer of the 102°-Hg_xTiS_2 structure. (b) Deintercalation begins with the formation of a GED termination at the right side of the gallery and TP stacking of the empty-gallery region. In (c) and (d) the gallery restacks via a $\frac{1}{2}\mathbf{b}$ shift together with a $\frac{1}{6}\mathbf{a}$ shift of the empty-gallery region to achieve octahedral TiS_2 coordination of the empty region In (c) the $\frac{1}{2}\mathbf{b}$ component of the interlayer shift is shown, including formation of the 96°-Hg_xTiS_2 phase in the intercalate region. In (d) the $\frac{1}{6}\mathbf{a}$ component of the restacking process, aided by asymmetric host-layer wrapping about the GED termination, results in octahedral coordination of the empty-gallery region to the right.

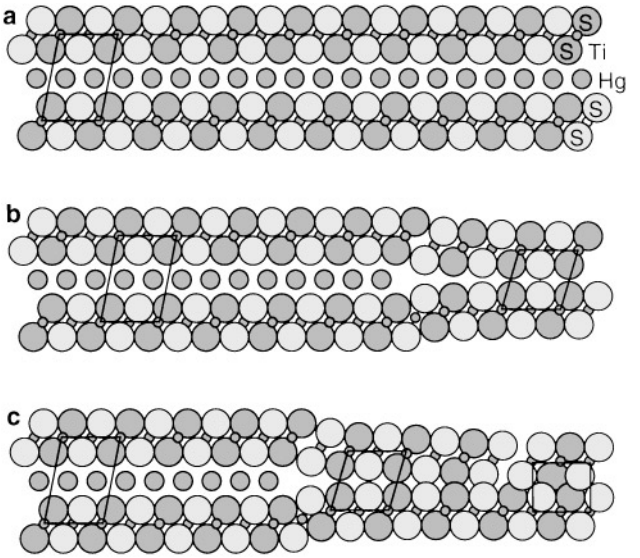

FIG. 6. A model of the delayed ($\frac{1}{2}\mathbf{b} + \frac{1}{6}\mathbf{a}$) deintercalation host-layer restacking process viewed along *b*. The arrangement in (a) shows a single intercalate layer of the 102°-Hg_xTiS_2 structure. (b) Deintercalation begins with the formation of a GED termination at the right side of the gallery and TP stacking of the empty gallery region. (c) Deintercalation proceeds with right-to-left motion of the GED termination accompanied by restacking of the right side of the empty-gallery region. DTAP ($\frac{1}{2}\mathbf{b}$) restacking of the right side of the empty-gallery region occurs, coupled with $\frac{1}{6}\mathbf{a}$ restacking in the far-right region to octahedral TiS_2 coordination. The strain induced along **a** to complete octahedral restacking of the far-right region causes the upper host layer to separate via an interlayer defect or crack.

Complex Restacking Mechanism with Defect Formation

As discussed previously, the restacking shift of the empty-gallery region can also be accomplished by a shift of $-\frac{1}{3}\mathbf{a}$, corresponding to a direct shift from the TP-coordinated intercalate region to an octahedrally coordinated empty-gallery region, without intermediate DTAP coordination. Such a restacking process would circumvent the generally observed 102°-to-96° Hg_xTiS_2 intercalate phase transition. It would also double the lamellar host-layer restacking shift for the intercalate-to-empty-gallery transition (perpendicular to the Hg chains) to 2 Å, resulting in substantially greater local elastic strain. Although evidence for this process has not been observed, it could possibly make a small contribution (e.g., resulting in occasional retention of 102°- Hg_xTiS_2 lamellae in matrices of the 96°-Hg_xTiS_2 intercalate) during deintercalation.

Another mechanism for defect formation is the delayed ($\frac{1}{2}\mathbf{b} + \frac{1}{6}\mathbf{a}$) restacking process suggested by Fig. 4 and schematically shown in Fig. 6. Such a process may also contribute to occasional retention of 102°-Hg_xTiS_2 lamellae in matrices of the 96°-Hg_xTiS_2 intercalate, as observed previously (11). In this process, the empty-gallery region again initially forms with TP coordination (Fig. 6b). However, instead of the entire gallery undergoing $\frac{1}{2}\mathbf{b}$ restacking early in the gallery deintercalation process, TP-intercalate and empty-gallery coordination are retained well into gallery deintercalation, perhaps due in part to relatively rapid deintercalation progression. The right side of the empty-gallery region eventually seeks energy minimization by beginning to restack to octahedral coordination. Initially, the onset of a $\frac{1}{2}\mathbf{b}$ shift at the right of the gallery begins, which is coupled with a $\frac{1}{6}\mathbf{a}$ shift via interlayer defect formation (i.e., nanocracking) to allow the right side of the gallery to achieve stable octahedral coordination. Such restacking defects could cause the crystallite cracking commonly observed during intercalation/deintercalation processes.

Unlike the $\frac{1}{6}\mathbf{a}$ shift across the 96°-Hg_xTiS_2-to-TiS_2 transition, the $\frac{1}{6}\mathbf{a}$ DTAP-to-octahedral shift across the empty-gallery region only involves a small decrease in

interlayer spacing (6.3 to 5.7 Å), which cannot readily accommodate significant interlayer restacking via asymmetrical bending of the gallery host layers. As a result, interlayer defects form to facilitate the restacking process.

CONCLUSIONS

The foregoing observations describe an overall deintercalation process in which individual intercalate lamellae independently undergo the 102°-to-96° Hg_xTiS_2 phase transition, stimulated by the onset of deintercalation in their associated galleries. Minimization of the elastic strain associated with gallery host-layer restacking provides the transition driving force. This process explains the observation of occasional $\frac{1}{2}\mathbf{b}$ shifts between host layers in *a*-axis HRTEM images of intercalated regions of partially deintercalated Hg_xTiS_2 (11). Such shifts originate from neighboring intercalate layers independently undergoing the 102°-to-96° phase transition.

Interlayer forces are known to play a role in the deintercalation process, which follows a general lamellar nucleation and growth mechanism (9). Deintercalation typically starts with both outermost and internal gallery onset, followed by gallery-by-gallery progression generally away from the onset galleries. The association of the lamellar 102°-to-96° Hg_xTiS_2 phase transition with the onset of individual gallery deintercalation suggests the transition exhibits similar nucleation and growth behavior, following in the footsteps of the gallery-by-gallery deintercalation process.

This is the first time the host-layer behavior governing individual gallery restacking mechanisms has been observed at the atomic level during deintercalation. This study has focused on the model-neutral Hg_xTiS_2 deintercalation process (4, 9), where the observed effects of elastic strain face minimal competition from electrostatic interlayer forces and result in the novel Hg_xTiS_2 deintercalation phase transition. The observed importance of elastic forces during intercalation/deintercalation processes, including phase transitions, should similarly extend to other intercalation systems (e.g., graphite) in which host-layer elastic deformation is an integral part of their intercalation and deintercalation processes. Similar studies for materials with stronger electrostatic interactions should provide new insight into the roles of elastic and electrostatic forces in deintercalation and intercalation processes.

ACKNOWLEDGMENTS

We acknowledge the National Science Foundation for support through Grant DMR 91-06792, and acknowledgment is made to the donors of the Petroleum Research Fund, administered by the American Chemical Society, for partial support of this research. The electron microscopy was conducted at the Center for High Resolution Electron Microscopy at Arizona State University, with partial support from NSF Grant DMR-9115680. We also thank the Center for Solid State Science for use of the Goldwater Materials Science Laboratories, including the Materials Facility.

REFERENCES

1. "Intercalated Layered Materials," F. Lévy, Ed., D. Reidel. Dordrecht, Holland, 1979.
2. "Intercalation Chemistry," M. S. Whittingham, A. J. Jacobson, Eds. Academic Press, New York, 1982.
3. E. W. Ong, Ph.D. Thesis, Arizona State University, Tempe, AZ, 1990.
4. M. McKelvy, R. Sharma, E. Ong, G. Burr, and W. Glaunsinger, *Chem. Mater.* **3,** 783 (1991).
5. E. W. Ong, M. J. McKelvy, G. Ouvrard, and W. S. Glaunsinger, *Chem. Mater.* **4,** 14 (1992).
6. P. Moreau and G. Ouvrard, *in* "Chemical Physics of Intercalation II" (P. Bernier, J.E. Fischer, S. Roth, and S. A. Solin, Eds.), NATO ASI Series Vol. 305, p. 351. Plenum Press, New York, 1993.
7. P. Ganal, W. Olberding, T. Butz, and G. Ouvrard, in "Chemical Physics of Intercalation II" (P. Bernier, J. E. Fischer, S. Roth, and S. A. Solin, Eds.), NATO ASI Series Vol. 305, p. 383. Plenum Press, New York, 1993.
8. P. Moreau, P. Ganal, and G. Ouvrard, *Mol. Cryst. Liq. Cryst.* **244,** 325 (1994).
9. M. McKelvy, M. Sidorov, A. Marie, R. Sharma, and W. Glaunsinger, *Chem. Mater.* **6,** 2233 (1994).
10. P. Ganal, P. Moreau, G. Ouvrard, M. Sidorov, M. McKelvy, and W. Glaunsinger, *Chem. Mater.* **7,** 1132 (1995).
11. M. Sidorov, M. McKelvy, R. Sharma, W. Glaunsinger, P. Ganal, P. Moreau, and G. Ouvrard, *Chem. Mater.* **7**, 1140 (1995).
12. P. Moreau, P. Ganal, S. Lemaux, G. Ouvrard, and M. McKelvy, *J. Phys. Chem. Solids* **57,** 1129 (1996).
13. M. J. McKelvy and W.S. Glaunsinger, *J. Solid State Chem.* **66,** 181 (1987).
14. A. H. Thompson, F.R. Gamble, and C.R. Symon, *Mater. Res. Bull.* **10,** 915 (1975).
15. W. J. de Ruijter, R. Sharma, M.R. McCartney, and D.J. Smith, *Ultramicroscopy* **57,** 409 (1995).
16. J. C. Russ, "The Image Processing Handbook." CRC Press, Boca Raton, FL, 1992.
17. R. R. Chianelli, J.C. Scanlon, and A.H. Thompson, *Mater. Res. Bull.* **10,** 1379 (1975).
18. N. Daumas and A. Hérold, *C. R. Seances Acad. Sci., Ser. C* **268,** 373 (1969).
19. G. Kirczenow, *in* "Graphite Intercalation Compounds I' (H. Zabel and S.A. Solin, Eds.), p. 59. Springer-Verlag, Berlin, 1990.